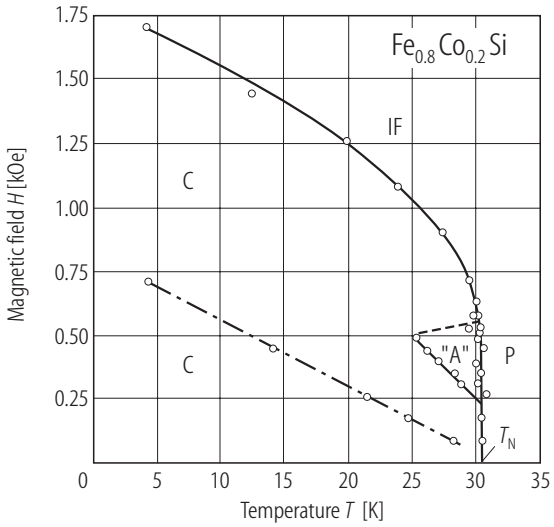

Fig. 91. $Fe_{0.8}Co_{0.2}Si$. Magnetic phase diagram in a magnetic field vs. temperature plane, as determined from magnetic measurements on a single crystal with the magnetic field H along the [110] direction. The compound has a helical spin structure for H = 0. C: conical arrangement of the spins; IF: field-induced ferromagnetism; P: paramagnetism; "A": unknown spin structure with a dip of magnetization. The chain line within the C region indicates a reorientation of the propagation vector of the cone-type magnetic structure to the direction of the applied magnetic field, when it is not along the field initially [90I1].

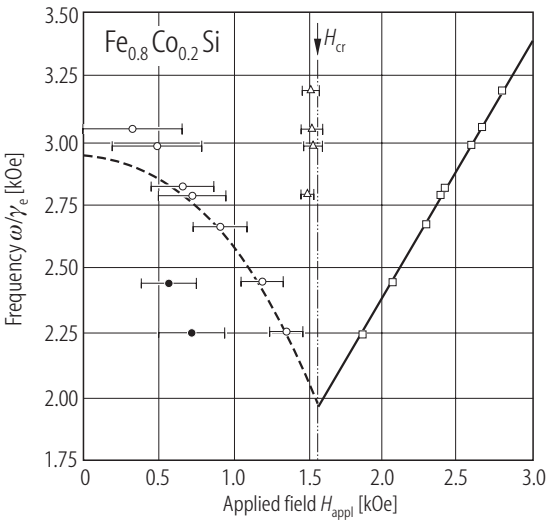

Fig. 92. $Fe_{0.8}Co_{0.2}Si$. ESR frequency ω/γ_e at 4.2 K plotted against the magnetic field applied, H_{appl}, along the [001] axis of a single crystal. H_{cr} is the critical field for induced ferromagnetic spin structure. The broken curve shows the theoretical curve for a helical spin resonance based on the antisymmetric exchange interaction of the Dzyaloshinski-Moriya type. The frequency is expressed in terms of ω/γ_e, the angular frequency divided by the magnetomechanical ratio of a free electron [89W1].

1.5.4.5.2 Alloys and compounds with Ge

The existence of two successive magnetic transitions in $FeGe_2$ has been established by [85C1] and the proposed collinear spin structure at lower temperature range seems to be supported theoretically [91G1], but it is still the subject of active discussion, because neither the anisotropy of magnetic susceptibility nor the magnetization curves in strong magnetic fields are consistent with the collinear spin structure [89Z1]. For the related ternary compound $Fe_{1-x}Co_xGe$ it is claimed [88P1] that crystal defects increase in the single-crystal specimens as x increases. This may lead to another complication for the physical properties of these compounds.

In the series of ternary compounds $Fe_{3-x}V_xGe$, doubly ordered cubic, $L2_1$ (Heusler alloy) type of crystal structure has been established through pulsed neutron powder diffraction at room temperature for x = 0.6, 0.8 and 1.0. The latter compound contains a small amount of undetermined second phase [90B1].

Survey

	Composition x	Properties	Figure	Table
$\alpha Fe_{1-x}Ge_x$	0.004...0.04	H_{hyp}(x) at ^{69}Ge	93	
$\gamma(Fe_{0.7}Mn_{0.3})_{1-x}Ge_x$	0...0.087	$\chi(T;x)$, T_N(x)	94, 95	
Fe_3Ge		a, c, H_{hyp}, ΔE_Q, IS		9

	Composition x	Properties	Figure	Table
Fe_5Ge_3		$\alpha(T)$	96	
FeGe (hex B35)		T-H magnetic phase diagram	97	9
FeGe (cub B20)		$I_{ND}(T)$, $I_{ND}(H)$	98, 99	9
$Fe_{7-x}Mn_xGe_6$	4	$\chi_g(T)$, $\chi_g^{-1}(T)$	100	
	0.5...4.5	T_N(x), Θ(x)	101	
$FeGe_2$		$C_p^{mag}(T)$	102	9
		$I_{ND}(T)$, $Q(T)$	103, 104	
$Fe_{1-x}Co_xGe_2$		$\chi_g(T;x)$	105	
		x-T magnetic phase diagram	106	

Table 9. Supplement to Table 10 in LB III/19C, subsect. 1.5.4.5.2. Magnetic and related properties of Fe_3Ge [85H1], hexagonal [88B1] and cubic [89L1] FeGe, and $FeGe_2$ [87D1].

	Fe_3Ge [1])	FeGe [3])	$FeGe_2$	
	T > 700 °C	metastable at T < 620 °C [67R1]	620 °C < T < 740 °C [67R1]	
Crystal structure	hexagonal $D0_{19}$ (Ni_3Sn)	hexagonal B35 (CoSn)	cubic B20 (FeSi)	tetragonal C16 ($CuAl_2$)
a [Å]	5.1806	5.003	4.689	5.908
c [Å]	4.2289	4.055		4.955
Magnetism	ferro	antiferro	helical	antiferro
T_N [K]		410	278.7 (first order)	290
p_{Fe} [μ_B/Fe]		1.38		
structure		60 K < T< T_N: collinear, $p_{Fe} \parallel c$ 30 K < T < 60 K: double cone, cone axis $\parallel c$ T < 30 K: similar to T > 30 K but with field-induced transitions by $H \perp c$	long-range spiral ($\lambda \approx 683…700$ Å) transition at T_{tr}: T_{tr} (down) = 211 K T_{tr} (up) = 245 K T_{tr} < T < T_N: Q = 0.0090 Å^{-1} $\parallel$ <100> T < T_{tr}: Q = 0.0092 Å^{-1} $\parallel$ <111>	first-order transition at T_{tr} = 263 K T_{tr} < T < T_N: $p_{Fe} \perp c$, incommensurate spiral $Q \parallel$ <100> T < T_{tr}: collinear $p_{Fe} \perp c$
H_{hyp} (^{57}Fe) [kOe]	260 at 10 K			
ΔE_Q (^{57}Fe) [mm s^{-1}]	0.06 at 10 K			
IS (^{57}Fe) [mm s^{-1}]	0.39 [2]) at 10 K			

[1]) No new data are available for low-temperature cubic Fe_3Ge and for ferromagnetism of hexagonal Fe_3Ge.
[2]) Relative to natural iron at RT. [3]) No new data are available for monoclinic FeGe stable at HT.

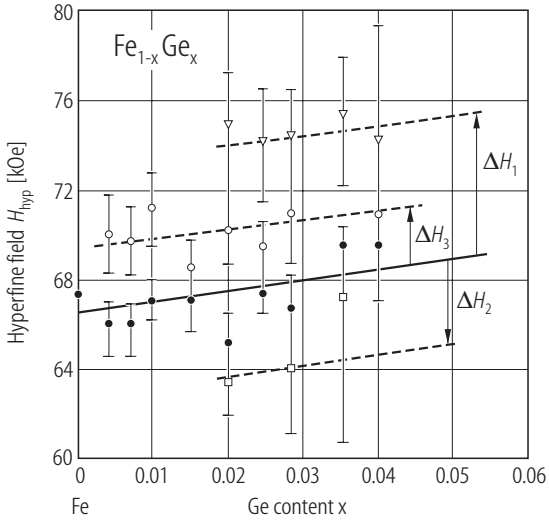

Fig. 93. Dilute $Fe_{1-x}Ge_x$ (αFe phase). Hyperfine field H_{hyp} at ^{69}Ge atom plotted against the Ge concentration. The hyperfine fields were determined by analyzing the data obtained by the time-differential perturbed angular distribution technique using the Ge isomer excited in heavy-ion reactions, and assigned as the contributions ΔH_i to the conduction-electron polarization from the first three (i = 1,2,3) nearest neighbours [91L1].

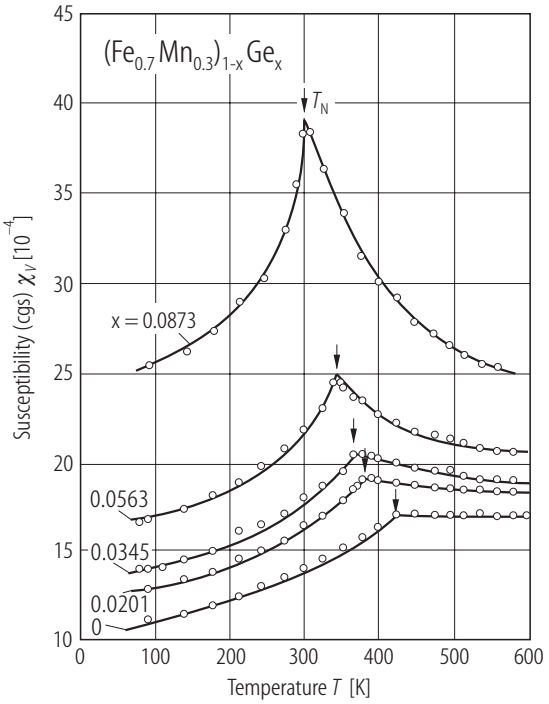

Fig. 94. $(Fe_{0.7}Mn_{0.3})_{1-x}Ge_x$ (γFe phase). Temperature dependence of the magnetic volume susceptibility χ_V, measured in a magnetic field of 4 kOe for various Ge concentrations [90Z1]. The compositions are nominal and a small amount (< 2 at%) of C is present.

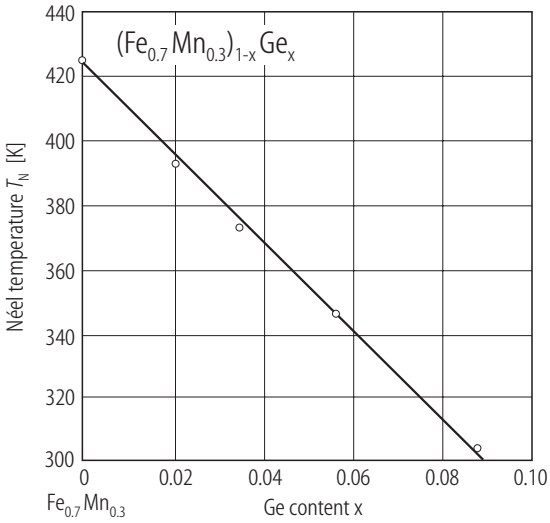

Fig. 95. $(Fe_{0.7}Mn_{0.3})_{1-x}Ge_x$ (γFe phase). Dependence of the Néel temperature T_N on the Ge concentration [90Z1], derived from the data of Fig. 94.

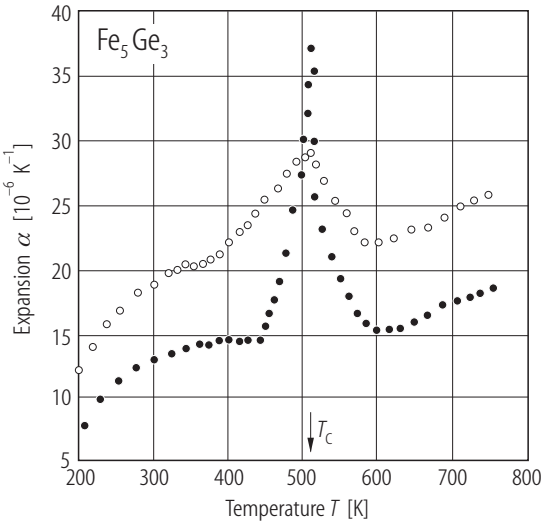

Fig. 96. Fe_5Ge_3, single crystal. Temperature dependence of the thermal expansion coefficient α. Solid circles: along *a* axis; open circles: along *c* axis [91M1].

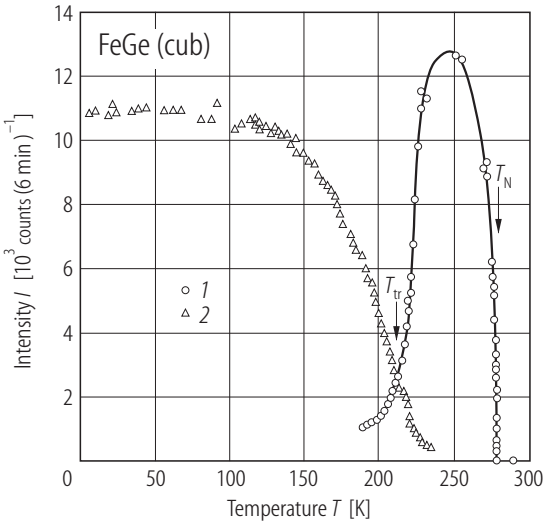

Fig. 98. FeGe (cubic, B20 type). Temperature dependence, for decreasing temperature, of the neutron integrated intensity I of the satellite lines around the (000), specifying the propagation vector of long-range helical arrangement of spins. (*1*): $-Q_0$[100] where Q_0 = 0.0090 Å^{-1}; (*2*): sum of $-(Q_0/\sqrt{3})(111)$ and $-(Q_0/\sqrt{3})(1\bar{1}\bar{1})$ where Q_0 = 0.0092 Å^{-1}. The transition at the Néel temperature T_N is inferred to be of first order with very little hysteresis, while the transition at T_{tr} with the change in the propagation vector shows pronounced hysteresis [89L1].

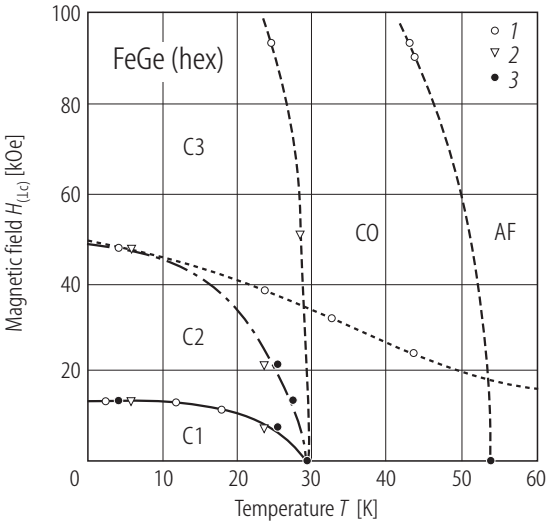

Fig. 97. FeGe (hexagonal, B35 type). Magnetic phase diagram in a temperature - magnetic field plane, as determined by neutron diffraction in magnetic fields applied perpendicular to the *c* axis [88B1]. AF: collinear antiferromagnetic along *c* axis; C0, C1, C2, C3: double cone antiferromagnetics with the axis of the cones along the *c* axis. The cone angle increases with decreasing temperature or increasing field. Transition between two C phases are characterized by a kink in the temperature dependence of the cone angle. (*1*) and (*2*): field-induced transitions detected in experiments with the applied fields along reciprocal-lattice vectors [100] and [1$\bar{2}$0], respectively; (*3*): transitions observed in earlier study [84B1]. Antiferromagnetic basal-plane moment appears above the dotted curve.

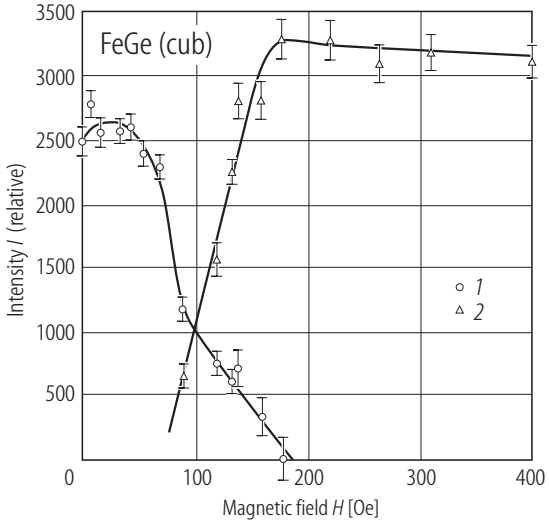

Fig. 99. FeGe (cubic, B20 type). Dependence at 250 K of the integrated intensity of specific satellites around (000) on the magnetic field along the [011] direction. (*1*): $\pm Q_0$ (100); (*2*): $\pm (Q_0/\sqrt{2})$ (011) appearing in the field direction above ≈ 80 Oe. Q_0 = 0.0090 Å^{-1} [89L1].

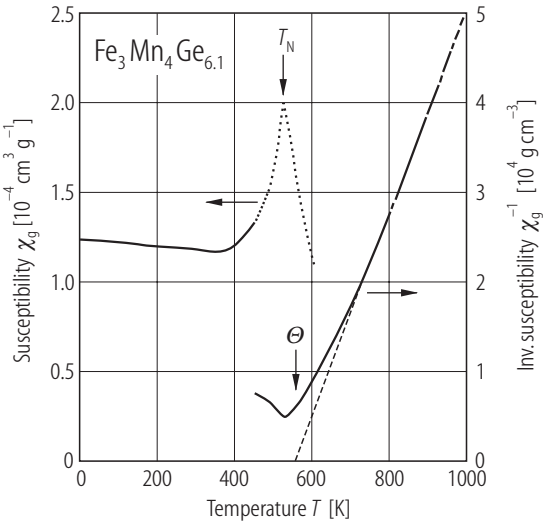

Fig. 100. $Fe_3Mn_4Ge_{6.1}$. Temperature dependence of the magnetic mass susceptibility χ_g and of its inverse, χ_g^{-1} [92H1].

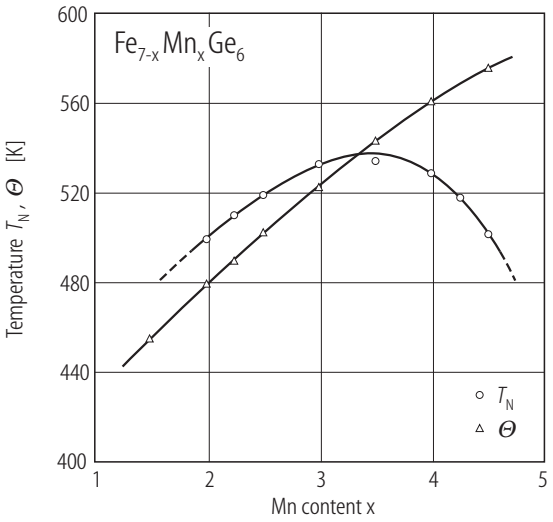

Fig. 101. $Fe_{7-x}Mn_xGe_6$. Composition dependence of the Néel temperature T_N and of the paramagnetic Curie temperature Θ [92H1].

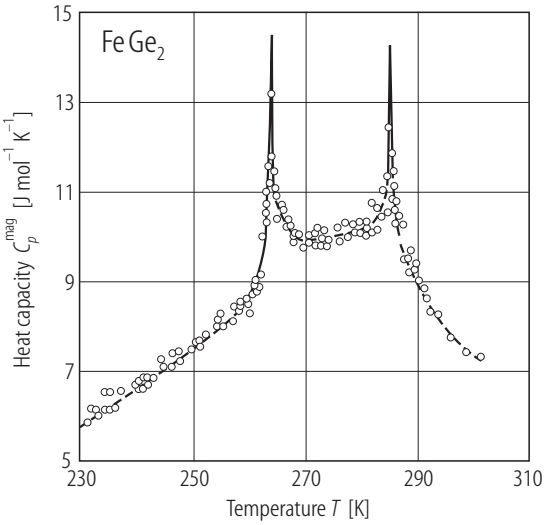

Fig. 102. $FeGe_2$. Temperature dependence of the magnetic contribution to the specific heat at constant pressure, C_p^{mag} [85C1].

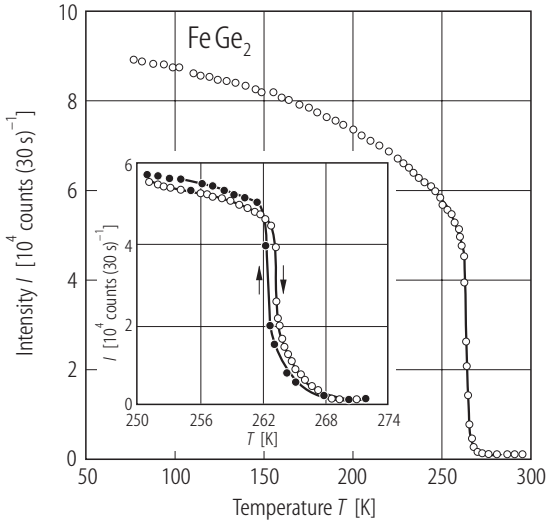

Fig. 103. $FeGe_2$. Temperature dependence of the neutron diffraction intensity I of the (100) magnetic reflection. Inset shows a thermal hysteresis of about 0.5 K [87D1].

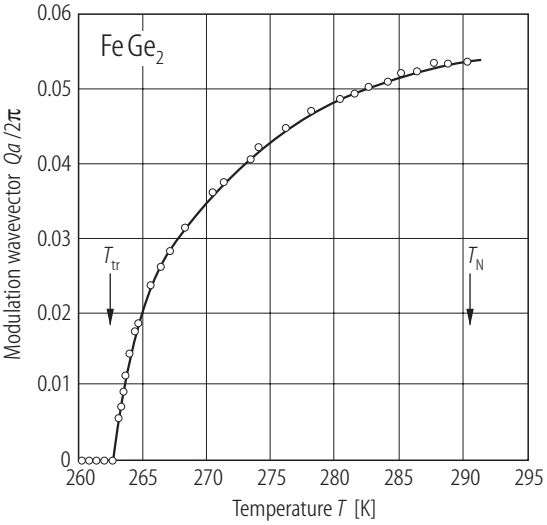

Fig. 104. $FeGe_2$. Temperature dependence of the magnitude of the propagation vector $\boldsymbol{Q}$ representing the incommensurate modulation of spin arrangement. $\boldsymbol{Q} \parallel$ <100> [87D1].

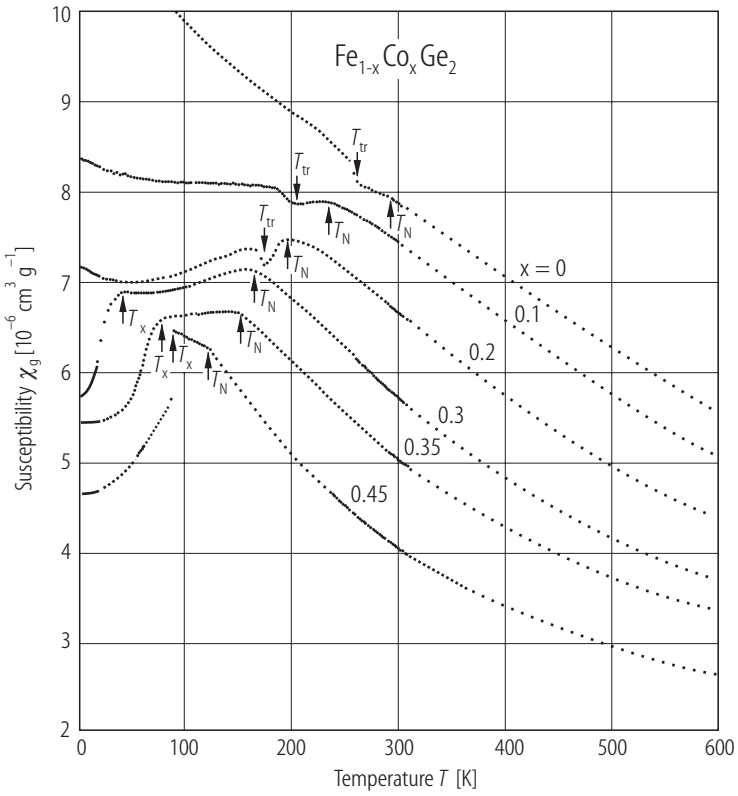

Fig. 105. $Fe_{1-x}Co_xGe_2$. Temperature dependence of the magnetic mass susceptibility χ_g in a magnetic field of 10 kOe. T_N: Néel temperature; T_{tr}: transition temperature to modulated spin structure; T_x: transition temperature of unknown origin [93S3].

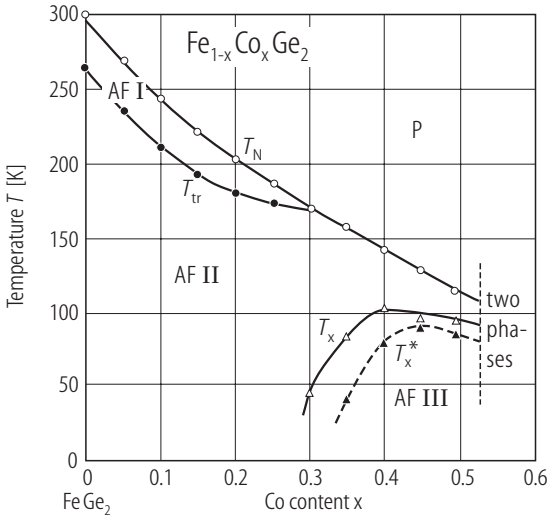

Fig. 106. $Fe_{1-x}Co_xGe_2$. Magnetic phase diagram in a composition - temperature plane, as obtained from magnetic measurements. AF I: antiferromagnet with modulated spin structure; AF II: with collinear structure; AF III: unknown structure. Magnetization curves of polycrystal specimens are linear below T_x^* and above T_{tr} [93S3].

1.5.4.5.3 Alloys and compounds with Sn

Magnetic structure of $FeSn_2$ has been re-investigated. Unfortunately, the single crystal specimen is very difficult to obtain, because $FeSn_2$ is formed through a peritectic reaction of FeSn and a Sn-rich liquid. The neutron-diffraction analysis has to be performed using powder specimens, leading to some ambiguity in the proposed magnetic structure.